sustainability

MDPI

Article

Numerical Study of Single-Layer and Stacked Minichannel-Based Heat Sinks Using Different Truncating Ratios for Cooling High Concentration Photovoltaic Systems

Ahmed T. Okasha [1], Fahad Ghallab Al-Amri [1,*], Taher Maatallah [1,*], Nagmeldeen A. M. Hassanain [1], Abdullah Khalid Alghamdi [1] and Richu Zachariah [2]

[1] Department of Mechanical and Energy Engineering, College of Engineering, Imam Abdulrahman Bin Faisal University, Dammam 34212, Saudi Arabia; ahmed.okasha1996@gmail.com (A.T.O.); nahassanain@iau.edu.sa (N.A.M.H.); abdullahkha.gh@gmail.com (A.K.A.)

[2] Department of Mechanical Engineering, Amal Jyothi College of Engineering, Kanjirappally 686518, Kerala, India; richuzachariah@gmail.com

* Correspondence: fgalamri@iau.edu.sa (F.G.A.-A.); tsmaatallah@iau.edu.sa (T.M.); Tel.: +966-504-955-412 (F.G.A.-A. & T.M.)

Abstract: The present research aims to discuss and analyze the performance of truncated single-layer and stacked mini-channel-based heat sinks employed for the cooling of a single-cell high concentrating photovoltaic systems. The truncating technique of the fins at the entrance and exit regions from the internal fluid mini channels is opted to reduce the energy, raw material costs and time of the manufacturing process of the mini channels. This proposed solution is constrained by several metrics such as the thermal management and the overall performance of the high concentrating photovoltaic system. In the current research, the use of a truncating ratio of 31% has yielded minimum cell temperature and maximum electrical efficiencies for both single-layer and stacked mini-channel-based heat sinks, while a truncating ratio of 65% has enabled more uniform cell temperature distribution. Moreover, a truncating ratio of 65% has qualified the highest water outlet temperature and the lowest pressure drops relatively compared to the conventional mini-channel-based heat sink configurations. The highest water temperature has reached up to 52.7 °C by the stacked mini-channel-based heat sink with a truncating ratio of 65% under a geometrical concentration ratio of 2000× and a mass flow rate of 0.001 kg s^{-1}. For both the single-layer and stacked mini-channel-based heat sinks, the use of a truncating ratio of 65% has driven the upper hands to achieve higher ratio of the thermal power to the pumping power (RTP). The maximum RTP values have been recorded by the single-layer mini-channel-based heat sink with a truncating ratio of 65% equal to 23.61 × 10^6 and 233.06 × 10^3 at a mass flow rate of 0.008 kg s^{-1} and 0.001 kg s^{-1}, respectively, under 2000×.

Keywords: high concentrated photovoltaic; mini channel-based heat sink; truncating ratio; thermal power to the pumping power ratio

check for updates

Citation: Okasha, A.T.; Al-Amri, F.G.; Maatallah, T.; Hassanain, N.A.M.; Alghamdi, A.K.; Zachariah, R. Numerical Study of Single-Layer and Stacked Minichannel-Based Heat Sinks Using Different Truncating Ratios for Cooling High Concentration Photovoltaic Systems. *Sustainability* **2022**, *14*, 5352. https://doi.org/10.3390/su14095352

Academic Editors: Md Shafiullah and Syed Masiur Rahman

Received: 19 March 2022
Accepted: 13 April 2022
Published: 29 April 2022

1. Introduction

Concentration photovoltaic (CPV) systems are expected to contribute a significant fraction of the renewable energy production in Saudi Arabia. This is due to the high Direct Normal Irradiance (DNI) in the Kingdom. In addition to that, CPV technology is well suited for the local manufacturing of a large percentage of the system's components to achieve the final products. Saudi Arabia aims to be a leading center for renewable energy within the next ten years, with a planned installed capacity of more than 58.7 GW (in which 2.7 GW will be produced by CPV technologies). It is a promising opportunity to meet the growing demand for energy resources and exploiting the favorable climatic conditions and appropriate economic feasibility [1,2].

Overheating the solar cells of the CPV systems can dramatically drop the overall CPV performance [3], especially in Saudi Arabia because during the hot season the ambient

temperature goes over 50 °C [4]. Hence, a sophisticated cooling technique must be carefully designed and adopted for CPV systems especially operating at high and ultra-high concentration levels (CR $\geq$ 100×) to ensure effective thermal management and optimum electrical efficiency. The concentration photovoltaic thermal (CPVT) systems can be used for various applications from generating electricity to fuels such as hydrogen [5,6].

Recently, several passive and active cooling setup and test rings have been employed to thermally manage the operation of the single-cell and densely packed High Concentration Photovoltaic (HCPV) modules. The cooling system can be selected according to the level of the concentration ratio (CR). There are two major cooling techniques of the CPV systems; the first one is the passive cooling, using heat sink, heat pipe, free air and phase change materials, while the active cooling uses flowing fluids (such as water or air) through channels, jet impingement, and mini channel and microchannel cooling methods [7–9]. It is worthiest to apply the passive cooling mechanism to dissipate heat and cool the solar cells under a CR less than 10×, as, depending usually on the weather conditions [10–12], increasing the convective heat transfer area can easily increase the dissipated heat rate and the solar cell efficiency. On the other hand, for High Concentration Ratios (100× $\leq$ CR $\leq$ 1000×) or Ultra-High Concentration Ratios (CR $\geq$ 1000×), using the active cooling techniques is more efficient to maintain CPV system temperature approximately constant over a long period under a wide range of Concentration Ratios (CR)s. Active cooling has better performance especially under harsh environmental conditions like that of Saudi Arabia [4,13,14].

The temperature limits of HCPV systems with mini channel cooling mechanism for Multi-Junction Solar Cell (MJSC) with a cell-active surface area of 10 × 10 mm^2 were investigated [13]. The applied CR was ranging between 500× to 2000× with three different cooling fluids. The solar cell temperature reached 93.5 °C, which means well below the maximum operating temperature of 110 °C at a mass flow rate of 6.74 × 10^{-4} kg s^{-1}. It was also demonstrated through this work that using water as a coolant fluid is the best choice for which the temperature distribution and the thermal efficiency were higher compared to other tested fluids.

The impact of the coolant properties on the electrical and thermal performance of different HCPV systems using the same MCBHS design and materials was studied [14]. Under the same heat sink dimensions and test conditions, the results demonstrated that the use of Nanofluids as coolant led to a maximum cell temperature of 95.25 °C and 67.1 °C, respectively, while the temperature difference over the solar cell was 35 °C under a CR of 2000× and at Reynolds number of 8.25 and 82.5. It has shown that the effectiveness of using Nanofluids has a very significant impact on HCPV thermal management.

The MCBHSs have many advantages over the other cooling techniques, and their thermal and hydraulic efficiencies have been studied through several recent research works [15–18]. A hybrid jet impingement was investigated experimentally to study the cooling effectiveness of the microchannel cooling under heat fluxes ranged between 21.8 W cm^{-2} and 32 W cm^{-2} [19]. A high concentration triple-junction solar cell was numerically investigated to compare two microchannel-based heat sink designs as cooling techniques [20]. The applied CR was 1000× and the configurations were examined using ANSYS Fluent software. Using a new convergent–divergent microchannel-based heat sink has a high heat transfer dissipation rate and cooling effectiveness compared to the conventional microchannel-based heat sink when the CR was ranged between 100× and 800× [21]. Passive and active cooling mechanism have been used to study different plate-fin channels and the flow inside them (copper–water nanofluid). The performance of the cooling methods have been experimentally investigated [22].

A high concentration triple-junction solar cell was numerically investigated and the thermal modeling was conducted using ANSYS Fluent to study the effect of two different active cooling mechanisms under 1000× [23,24]. Four differently shaped microchannel-based heat sinks were used for heat transfer optimization of a high single-solar cell CPV module [25]. The design was tested numerically without the introduction of the jet impingement cooling technique. A CPV system that consists of four solar cells connected thermally

at the top to a copper tube is investigated [26]. The system was tested with two different tubes having the same outer diameter. Ultra-High Concentration Photovoltaic (UHCPV) systems are highly recommended to reduce the semiconductor materials and to maximize the output power at high electrical conversion efficiencies.The performance of the UHCPV systems is limited by the extreme unwanted high cell temperature that could be achieved at high solar projected power on the solar cells. Indeed, there are many techniques to decrease the thermal resistance toward higher cooling effectiveness and capacity to extract the maximum of the heat from the solar cell domains. An appropriate heat sink design using multiple channel configurations with various fin heights and thicknesses has been studied and optimized to reduce the UHCPV surface cell temperature [27] via Ansys Fluent software under a CR of 1800×. The active UHCPV cell area is 100 mm^2.

Using internal fluid mini-channel-based heat sink is one of the most practical and convenient solutions to reduce the thermal resistance of the HCPV and UHCPV systems and record optimum overall efficiencies; however, the increase in the power consumption of the micro-pump driving the coolant flow reduces the net output power and cost-effectiveness of the system, besides the high required energy and manufacturing costs of the single-layer or stacked mini channels. In effect, conventional manufacturing techniques such as forging, mold casting, die casting or plastic injecting cannot manufacture such small and complicated shaped MCBHS. A mini channel can be manufactured by two commercially available sophisticated techniques: subtracting and additive manufacturing processes. The subtracting processes, using for example the five-axis Computerized Numerical Control (CNC) machine (for turning, drilling, milling and grinding) may experience major difficulties in manufacturing products with internal fluid channels and this result usually in scarifying some functional performance or add extra unnecessary weight to meet manufacturing feasibility because especially the internal mini or micro channels are highly complicated due to their very small sizes. The additive manufacturing technology, termed also the 3D-metal printing process, has shown higher performance thanks to its production process automation and high degree of design freedom; however, to date no state-of-the-art of the 3D-metal printing manufactured products with internal fluid channels is present. Moreover, this technique consumes much time and materials. Thus, any modifications in the design that lead to reducing the complexity or the required material will save enormous time and cost during the fabrication of the mini channels.

In the present paper, without taking into account the optimal dimensions of the fins (thickness and length) and their wise spacing, the performance of the single-layer and stacked (four-layers) mini-channel-based heat sinks (MCBHS) with two truncating ratios at the entrance and the exit regions from the mini channel are investigated and discussed. In the present study, two appropriate truncating ratios of 65% and 31% have been considered. The influence of removing (or truncating) an appropriate fraction or ratios from the fins at the entrance and exit of the finned mini channels is targeted toward lower weight of the MCBHS (which is very valuable for the tracking energy cost), reduced energy cost and required raw materials for the manufacturing process of the MCBHS, and higher net output power of the HCPV modules. This aim may be constrained by the thermal management and overall performance of such cooling technology. Therefore, the main objective of the present work is to comprehensively study the influence, if there is, of truncating the non-effective fins-ratio at the entrance and exit of the single and stacked mini channels on the functionalities of the MCBHS and the overall HCPV performance.

2. Design and Methodology

2.1. Conceptual Design

In the present study, the influence of the truncating ratio of the heat sink area is numerically investigated to end up with an enhanced cooling mechanism of the HCPV modules relatively compared to the existing designs. The effects of removing an appropriate ratio (truncating ratio) from the fins at the entrance and exit regions of the single-layer and stacked MHSC (with four layers), that have never been studied, will be assessed and

discussed based on different performance metrics. In the present study, all the investigated configurations have parallel directions. The effect of the number of the mini channel layers and the flow direction are not studied in the present work, however they have also particular interest for the avenue and the further development of the present research. Moreover, the four-layered mini channel is the stacked mini channel arrangement that has been considered in the current research.

The three-dimensional layouts of the conventional single-layer and stacked MCBHS are shown in Figures 1 and 2, respectively. For each heat sink layer, the length, width and height is 29, 27 and 6 mm, respectively, and the total number of fins and water channels is 26 and 27, respectively. These dimensions have been selected for the sake of comparison against the results obtained by Ahmed et al. [13]. Therefore, an identical geometry of the single-layer MCBHS was adopted to ensure fair and accurate numerical validation. For the baseline configuration, each heat sink substrate has a size of 783% relatively compared to the size of the cell, while the flow channels area is extended by 67.5% in the direction of the flow and 94.5% in the direction perpendicular to the flow. For the conventional stacked MCBHS, the flow channels area is extended by 43.75% in the direction of the flow and 114.75% in the direction perpendicular to the flow, relatively compared to the size of the solar cell.

Figure 3 depicts the first two proposed configurations: single-layer and stacked MCBHS design with a truncating ratio of 65%. In effect, in these two configurations, 65% of the fins are removed, while keeping those just under the solar cell (35%). Figure 4 represents the third and fourth studied configurations: single-layer and four-layers MCBHS designs with a truncating ratio of 31%; only the fins at the inlet and exit regions are removed.

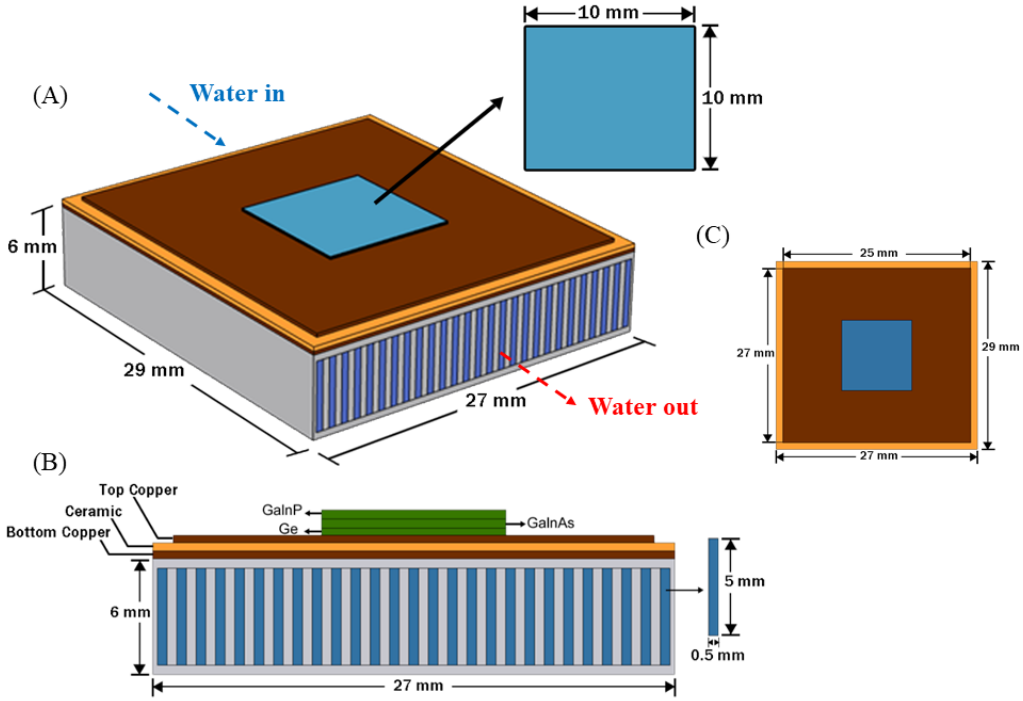

Figure 1. Geometric model of the conventional finned aluminum MCBHS: (**A**) isometric view, (**B**) side view and (**C**) top view.

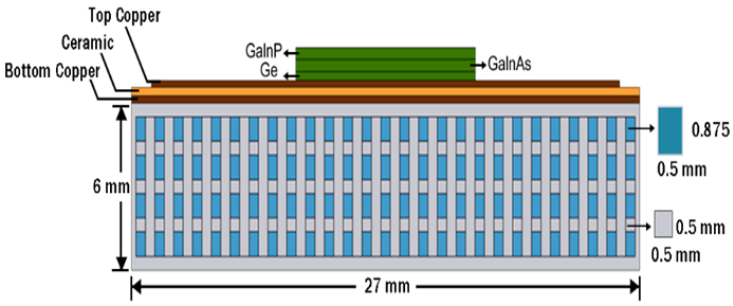

Figure 2. Geometric model of the conventional stacked MCBHS design.

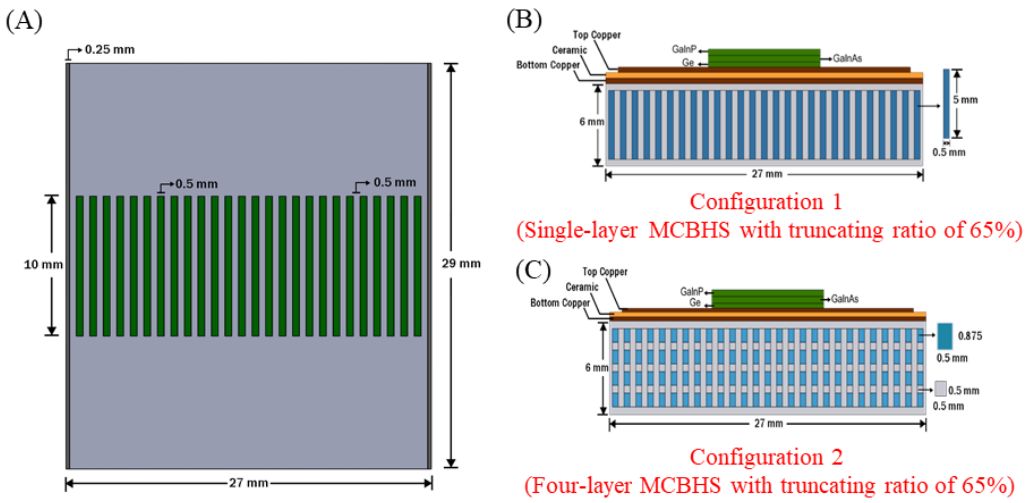

Figure 3. Geometric model of the MCBHS design with a truncating ratio of 65%: (**A**) top view and (**B**) side view of single-layer MCBHS design (configuration 1); (**C**) side view of stacked MCBHS design (configuration 2).

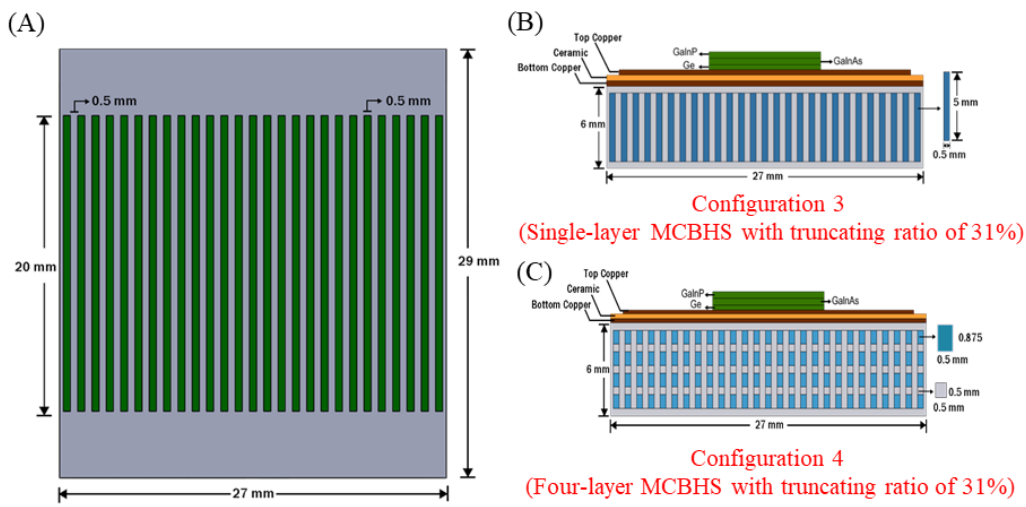

Figure 4. Geometric model of the MCBHS design with a truncating ratio of 31%: (**A**) top view and (**B**) side view of single-layer MCBHS design (configuration 3); (**C**) side view of stacked MCBHS design (configuration 4).

2.2. Simulation Setup

The simulations were conducted on a CPU with 8.00 GHz and 16.0 GB of RAM capacity. For the numerical simulation, COMSOL Multiphysics® Version 5.6 is used to

resolve the conjugate laminar flow–heat transfer model. First, grid independence analysis was performed to select the accurate grid size ensuring stable and convergent numerical solutions. Then, the validation of the numerical model were accomplished.

2.3. Governing Equations, Boundary Conditions, and Assumptions

2.3.1. Governing Equations

The flow inside the channel is modeled using Navier–Stokes equations. The governing equations describing the fluid domain can be written as the following [28,29]:

The continuity equation is written as follows:

$$\nabla \cdot (\rho \vec{v}) = 0 \tag{1}$$

The momentum conservation equation is:

$$\nabla \cdot (\rho \vec{v}\vec{v}) = -\nabla p + \nabla \cdot (\overline{\overline{\tau}}) + \rho \vec{g} \tag{2}$$

where $\rho \vec{g}$ is the gravitational body force.

The viscous stress tensor can be described by:

$$\overline{\overline{\tau}} = \mu\left(\nabla \vec{v} + (\nabla \vec{v})^T\right) - \frac{2}{3}\mu(\nabla \cdot \vec{v})I \tag{3}$$

The energy equation can be written as:

$$\nabla \cdot (\rho \vec{v} E) = -\nabla(k \cdot \nabla T) + \nabla \cdot (\vec{v} \cdot \overline{\overline{\tau}}) \tag{4}$$

2.3.2. Overall Single-Cell HCPV Module Efficiency

The energy transfer through the UHCPV system is illustrated in Figure 5. The UHCPV module consists of MJSCl (1) cell Germanium (Ge), (2) Indium Gallium Phosphide (GalnP), (3) Indium Gallium Arsenide (GalnAs), Copper layers, Ceramic layer and the MCBHS. The total input power from the incident solar irradiance can be calculated as follows [30]:

$$Q_{\text{in}} = DNI \cdot CR \cdot \eta_{\text{opt}} \cdot A_{\text{cell}} \tag{5}$$

where A_{cell} is the active cell surface area.

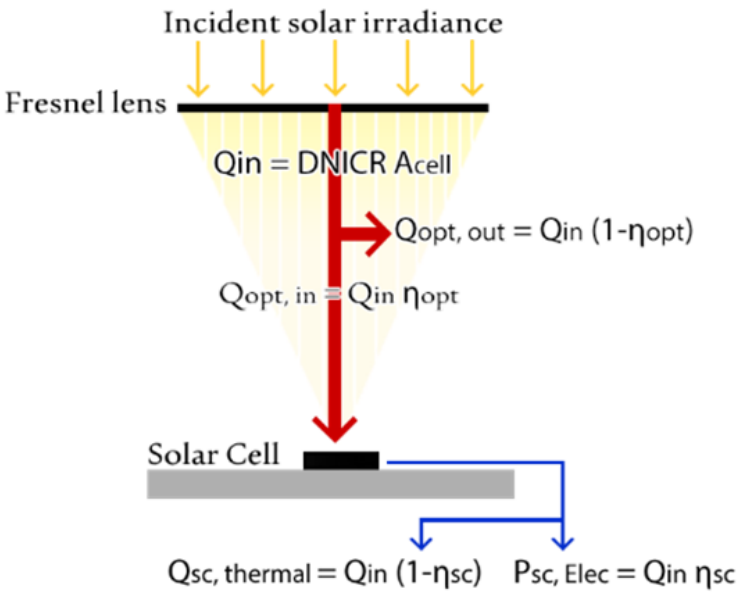

Figure 5. Energy transfer through the UHCPV system.

Part of the input power is then converted to electrical power, $P_{sc,elec}$, while the rest is converted into a thermal power, Q.

$$P_{sc,elec} = Q_{in} \cdot \eta_{sc} \tag{6}$$

$$Q = Q_{in} \cdot (1 - \eta_{sc}) \tag{7}$$

The heat power of the cooling, Q_{th}, is the amount of heat that is transferred per unit of time to the coolant and can be expressed as follows:

$$Q_{th} = \dot{m} \cdot C_p \cdot (T_{f,out} - T_{f,in}) \tag{8}$$

where, $\dot{m}$ is the mass flow rate (kg s^{-1}) and C_p is the specific heat capacity (J kg^{-1} K^{-1}) of the fluid. The thermal efficiency, η_{th}, is expressed as the following:

$$\eta_{th} = \frac{Q_{th}}{Q_{in}} \times 100 \tag{9}$$

The overall HCPV system efficiency can be described as follows:

$$\eta_{overall} = \frac{Q_{th} + P_{elec,net}}{Q_{in}} \times 100 \tag{10}$$

The pumping power can then be formulated as:

$$P_{pump} = \dot{V} \cdot \Delta P \tag{11}$$

where ΔP is the pressure drop inside the channel (Pa) and $\dot{V}$ is the volume flow rate of the fluid (m^3 s^{-1}).

2.3.3. Boundary Conditions and Assumptions

To solve the above-mentioned equations (continuity, momentum and energy equations), the following boundary conditions and assumptions are applied (Figure 6):

1. The boundary heat source is applied to the germanium layer.
2. The top surfaces, i.e., copper layer, ceramic layer and cell top surface, are subjected to the natural convection with a constant heat transfer coefficient of (h = 15 W m^{-2} K^{-1}) and surface to ambient heat transfer radiation.
3. Thermo-physical properties of the water have temperature-dependent values.
4. The sided walls and the back plate of the MCBHS are insulated to minimize the heat losses to the surroundings.
5. The ambient and inlet water temperatures were assumed equal to 25 °C.
6. The range of inlet water mass flow rate in each channel is set to be between 0.001 kg s^{-1} and 0.008 kg s^{-1}.
7. The water flow is assumed laminar, steady and incompressible.
8. The active cell surface area is 10 × 10 mm^2.
9. Reynolds number range is 7–508.
10. CR is ranged between (500×–2000×).

The dimensions and thermal properties of the solar cell and heat sink are recapitulated in Tables 1 and 2.

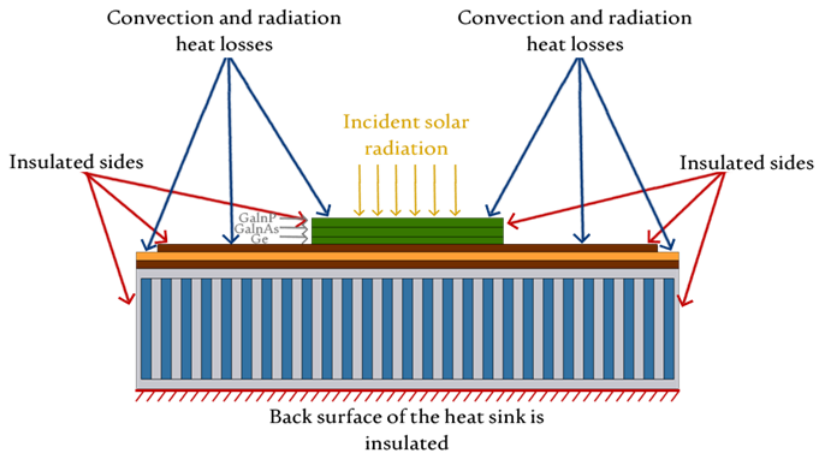

Figure 6. Schematic diagram of the boundary conditions of both the HCPV system and the attached heat sink.

Table 1. Dimensions of the HCPV layers.

Material	Length (mm)	Width (mm)	Thickness (mm)
Aluminum	29	27	6
GaInP	10	10	0.07
GaInAs	10	10	0.07
Ge	10	10	0.07
Copper (1)	27	25	0.25
Ceramic	29	27	0.32
Copper (2)	29	27	0.25

Table 2. Thermo-physical properties of the used materials.

Material	Thermal Conductivity, k (W m^{-1} K^{-1})	Specific Heat Capacity, C (J kg^{-1} K^{-1})	Density, ρ (kg m^{-3})	Emissivity, ϵ
Aluminum	160	900	2700	-
GaInP	73	370	4470	0.9
GaInAs	65	550	5316	-
Ge	60	320	5323	-
Copper	400	385	8700	0.05
Ceramic	27	900	3900	0.75

2.3.4. Mesh Independence Study

The simulations were conducted on a CPU with a 8.00 GHz and 16.0 GB of RAM capacity. The simulation was performed using COMSOL Multiphysics Version 5.6.A grid independence study was performed to ensure the accuracy of the model outcomes. For each configuration, a test grid independence study was applied to select the mesh that comprises the minimum number of elements ensuring stable and convergent solutions. Figure 7A shows the maximum solar cell temperature variation of the HCPV module that integrates the conventional mini-channel-based heat design against the mesh element size, which is varied from 0.177×10^6 to 14×10^6 tetrahedral elements. As shown in Figure 7A, the maximum cell temperature becomes constant for a mesh of size higher than 3.2 million elements. To reduce the model computational time, the mesh of 3.2 million tetrahedral elements is selected and applied to the UHCPV domains, as generated, and depicted in Figure 7B.

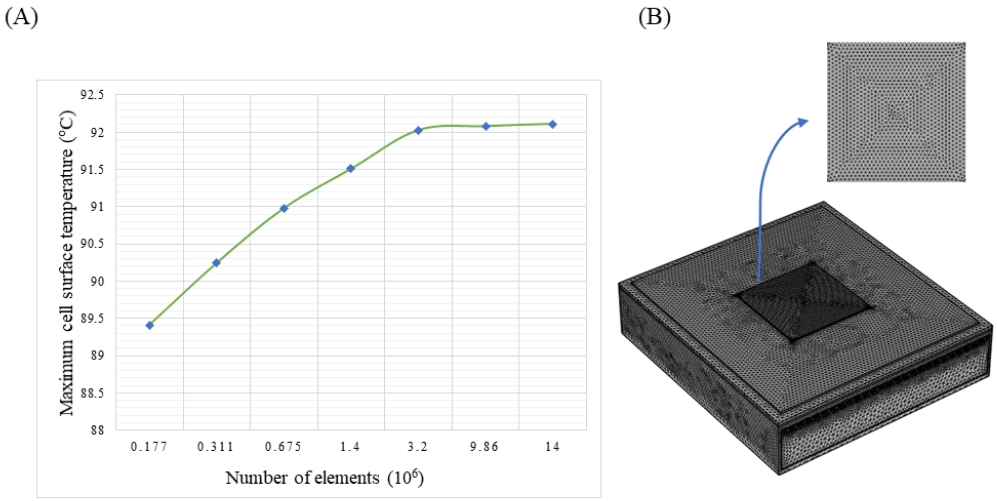

Figure 7. (**A**) Mesh independence study for the maximum cell surface temperature at CR = 2000× and mass flow rate of 0.001 kg s^{-1} for the first configuration. (**B**) The generated mesh.

2.3.5. Validation Study

The obtained numerical results were compared to those of Ahmed et al. [13] to validate the accuracy of the developed model. Figure 8 shows the trending of the maximum cell temperature at different mass flow rates assuming identical HCPV module dimensions, thermophysical properties and boundary conditions. The present model has fitted closely the baseline results of Ahmed et al. [13], where the maximum mean relative error between the recorded maximum cell temperature was about 1.6%.

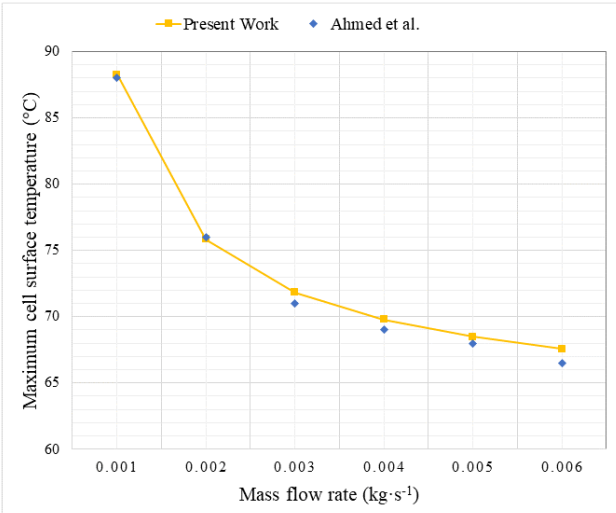

Figure 8. Variation of the solar cell maximum temperature against different water flow rates for the work of Ahmed et al. [13] and the present work.

3. Results and Discussion

In this section, the influence of the truncating ratio and the mass flow rate at a wide range of geometrical concentration ratios on the maximum cell temperature, temperature uniformity, electrical efficiency, pressure drop and the ratio of the thermal power to the pumping power of each configuration from each design have been analyzed and discussed.

3.1. Maximum Solar Cell Surface Temperature and Temperature Uniformity

Figure 9 depicts the profile of the maximum surface MJSC temperature at different mass flow rates, ranging between 0.001 kg s^{-1} and 0.008 kg s^{-1} under CRs varied between 500× and 2000×. It was found that, for both the single-layer and stacked MCBHS, the minimum surface MJSC temperature was achieved using a truncating ratio of 31%. The bottom boundaries of the heat sink on the removed sides are insulated, which explains the colder water temperature reaching the solar cell surface area being located at the center of the heat sink surface area. Consequently, a higher temperature gradient between the solar cell and the water flux is achieved, ensuring a better heat extraction rate and lower solar cell temperature. Therefore, removing 31% from the fins at the entrance and exit of the mini channel has yielded the lowest cell temperature, and a gain of 31% of the required materials and manufacturing cost.

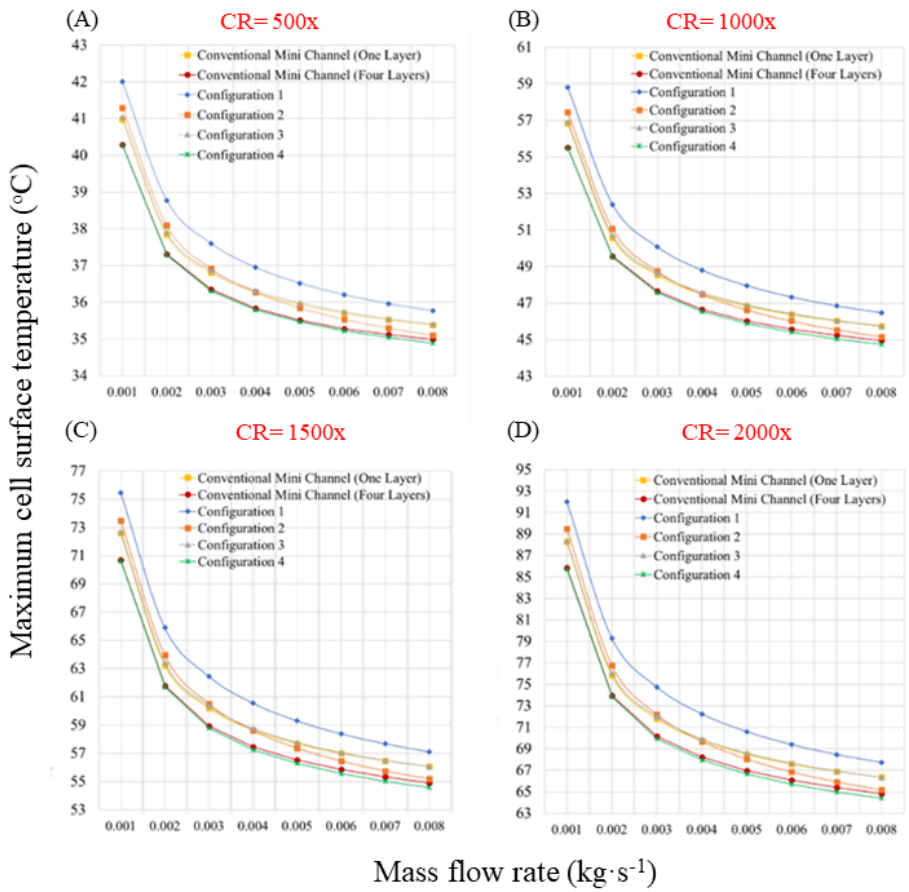

Figure 9. Variation of the cell maximum surface temperature vs. mass flow rate for all MCBHSs under: (**A**) 500× (**B**) 1000× (**C**) 1500× and (**D**) 2000×.

A truncating ratio of 65% was seen not effective for reducing the maximum cell temperature compared to the conventional configurations and the MCBHS with a truncating ratio of 31%. When removing a fins ratio of 65%, higher cell temperatures were observed since the increment in the bulk and conduction thermal resistances at the entrance and exit regions had overcome the extra-convective heat transfer rate resulted in colder water flow flowing below the solar surface area. The cell temperature reached SI 85.8 °C, 89.4 °C, and 85.7 °C under CR of 2000× and mass flow rate of 0.001 kg s^{-1} for the conventional four-layered MCBHS, stacked MCBHS with a truncating ratio of 65% and stacked MCBHS with a truncating ratio of 31%, respectively.

On the other hand, it was clear that the increase of the mass flow rate reduces the maximum surface MJSC temperature, allowing more heat being extracted from the solar cell domain. For instance, at a water mass flow rate of 0.008 kg s^{-1}, the maximum cell

temperature has been significantly reduced to 34.8 °C for the fourth configuration at a CR of 500×.

Figure 10 displays the temperature difference over the solar cell (difference between the maximum and minimum cell temperature) at various mass flow rates under 2000×. It is clear that for both single-layer and stacked MCBHS, a truncating ratio of 65% is more effective to ensure more surface temperature uniformity. The second configuration (stacked MCBHS with a truncating ratio of 65%) has the most uniform temperature distribution followed by the first, fourth, and third configuration. The conventional single-layer MCBHS design corresponded to the worst scenario with a cell temperature increase of 6.2 °C and 2.6 °C at a mass flow rate of 0.001 kg s^{-1} and 0.007 kg s^{-1}, respectively, relatively compared to the stacked MCBHS with a truncating ratio of 65%. The temperature difference over the cell for the latter design was ranged between 25.8 °C and 21.7 °C, at flow rates ranging from 0.001 kg s^{-1} to 0.007 kg s^{-1}, respectively.

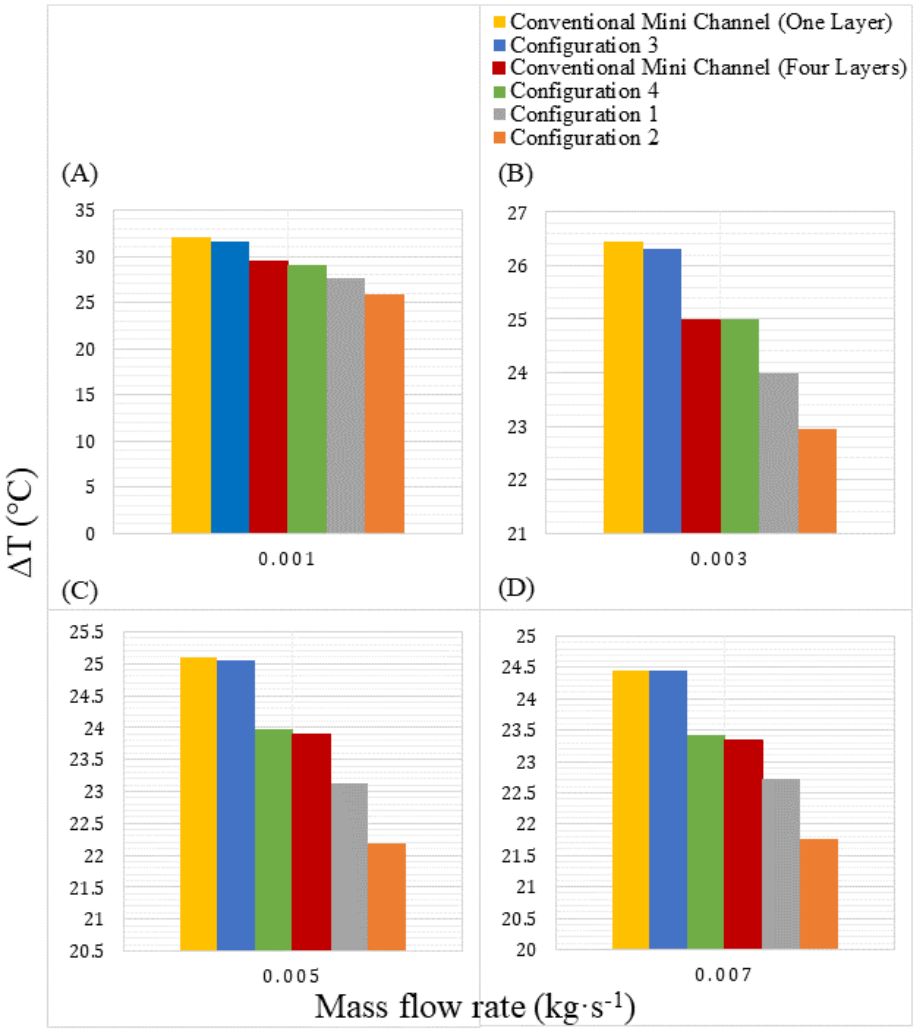

Figure 10. Temperature difference within the MJSC for all MCBHSs under CR = 2000× at: (**A**) 0.001 kg s^{-1}, (**B**) 0.003 kg s^{-1}, (**C**) 0.0075 kg s^{-1} and (**D**) 0.007 kg s^{-1}.

3.2. Water Outlet Temperature

Figure 11 represents the variation of the water outlet temperature for several mass flow rates, ranging between 0.001 kg s^{-1} and 0.008 kg s^{-1} and under CR varying from 500× to 2000×. It was perceived that despite of the difference in the overall thermal resistance of the investigated configurations, the outlet temperature in each channel was the same. The results showed that no one among the six studied MCBHS configurations has the

upper hands to achieve higher temperature over the other ones, and then further thermal energy utilization at the downstream of the HCPV module. This closed water outlet temperature ranges is explained by the fact that, since the heat capacity of water is high, the distinct recorded thermal resistance by the different studied configurations can lead only to insignificant increase in their temperature. However, the range of the outlet water temperature for the smallest water flow rates can be useful for a wide range of applications, such as membrane desalination, water heating and air conditioning. To be specific, the outlet temperature is within the recommended hot feed-in water temperature range of 50 °C to 70 °C for air–gap membrane desalination [31,32]. Most home and commercial activities, such as bathing, washing and cleaning, require hot water temperatures ranging from 50 °C to 60 °C [33]. In addition, hot water with a temperature higher than 50 °C can be used as a heat source for adsorption cooling systems [34]. Moreover, it is observed that increasing the mass flow rate decreases the outlet temperature. Indeed, the highest water outlet temperature was recorded by the stacked MCBHS with a truncating ratio of 65% for all configurations and reached up to 52.7 °C and 32 °C, under CR of 2000× and 500×, respectively, at a mass flow rate of 0.001 kg s^{-1}.

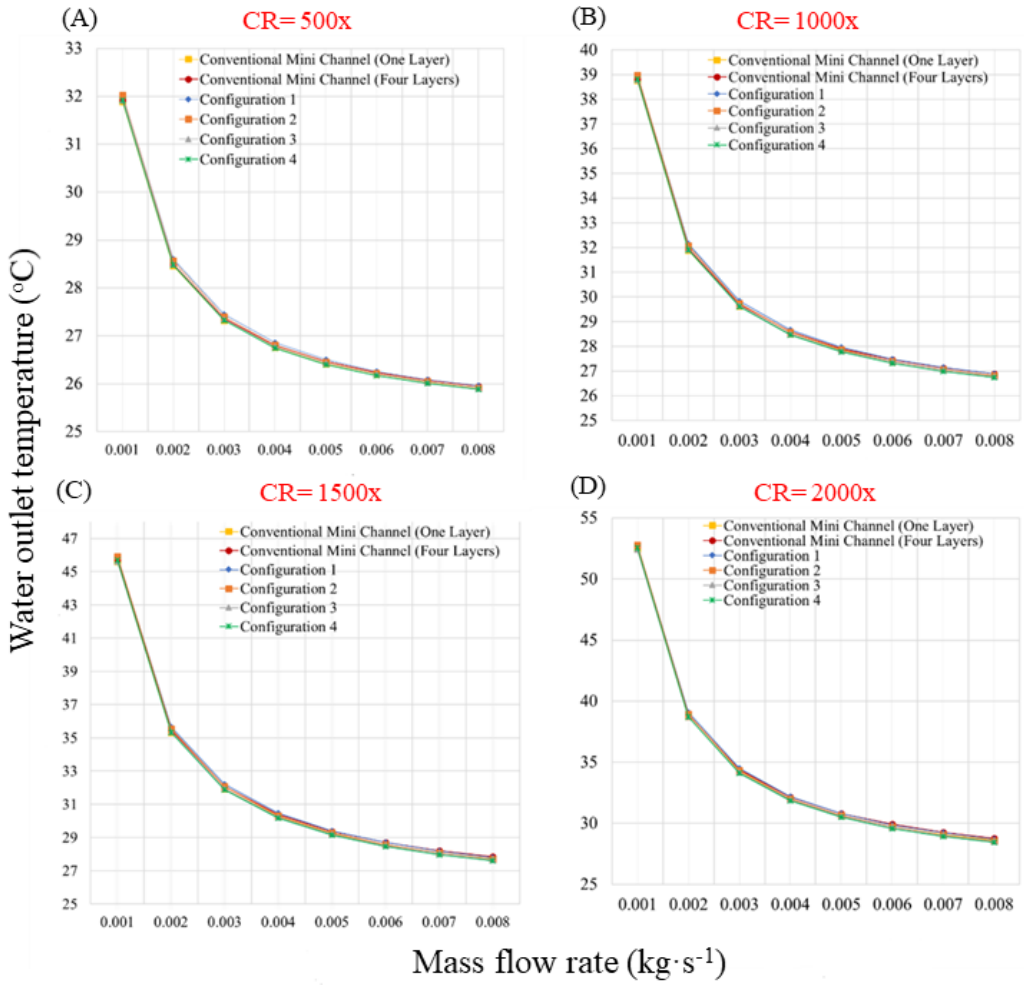

Figure 11. Variation of the water outlet temperature as function of mass flow rate at: (**A**) 500×, (**B**) 1000×, (**C**) 1500× and (**D**) 2000×.

3.3. Electrical Efficiency

Figure 12 depicts the electrical efficiency variation for all MCBHS configurations. It shows that the highest electrical efficiency was achieved by the fourth configuration (stacked MCBHS with a truncating ratio of 31%) reaching the value of 40.05% at a mass

flow rate of 0.008 kg s^{-1} and CR of 500×. As shown in Figure 12, the electrical efficiency decreased by increasing the CR as a large amount of the incident solar power is converted into heat. On the other hand, the electrical efficiency has a proportional relationship with the mass flow rate. For the best-case scenario (Configuration 4) the electrical efficiency decreased with a minor effect once compared to the conventional single-layer MCBHS design by a maximum of 1.24% at a mass flow rate of 0.001 kg s^{-1}, especially at CR of 2000×.

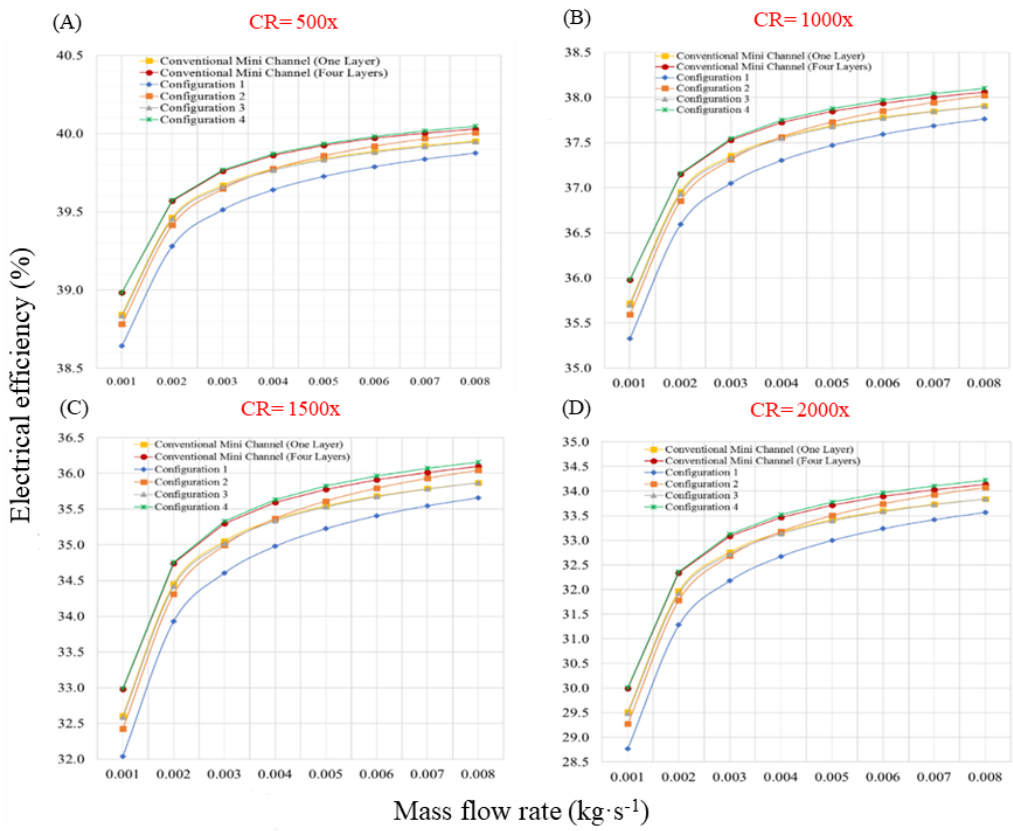

Figure 12. Variation of the electrical efficiency with mass flow rates under CR of: (**A**) 500× (**B**) 1000× (**C**) 1500× and (**D**) 2000×.

3.4. Pressure Drop

The pressure drop is a key design parameter that must be carefully considered in active cooling systems and more specifically for MCBHSs. In effect, increasing the mass flow rate leads to a dramatic increase in pressure drop which requires high pumping power and causes a drop in the net output power and the overall exergetic efficiency of the HCPV module. Furthermore, a mini channel stack eventually requires less pumping power to remove a given heat load than a single-layered mini channel, because it provides a larger heat transfer area. Thus, an optimal design for one set of parameters does not mean that it is optimal for another set of ones. To optimize the overall functionalities of a mini-channel-based heat implies considering the cost energy of manufacturing, the required materials of fabrications and the required pumping power under a prescribed operating conditions. In the current research, the mini channel design is not constrained by a fixed pressure drop threshold; however, the optimal designed will be identified based on a designless analysis. From another perspective, the overall thermal resistance can be reduced by increasing the pumping power or employing short channels. Figure 13 shows the pressure drop at various mass flow rates under 500×. It was observed that the pressure drop in each channel is the same, irrespective of the number of layers. A truncating ratio of 65% qualifies the recording of the minimum pressure drops relatively compared to the

conventional MCBHS configurations. The conventional stacked MCBHS configuration shows the highest pressure drop among all the studied configurations.

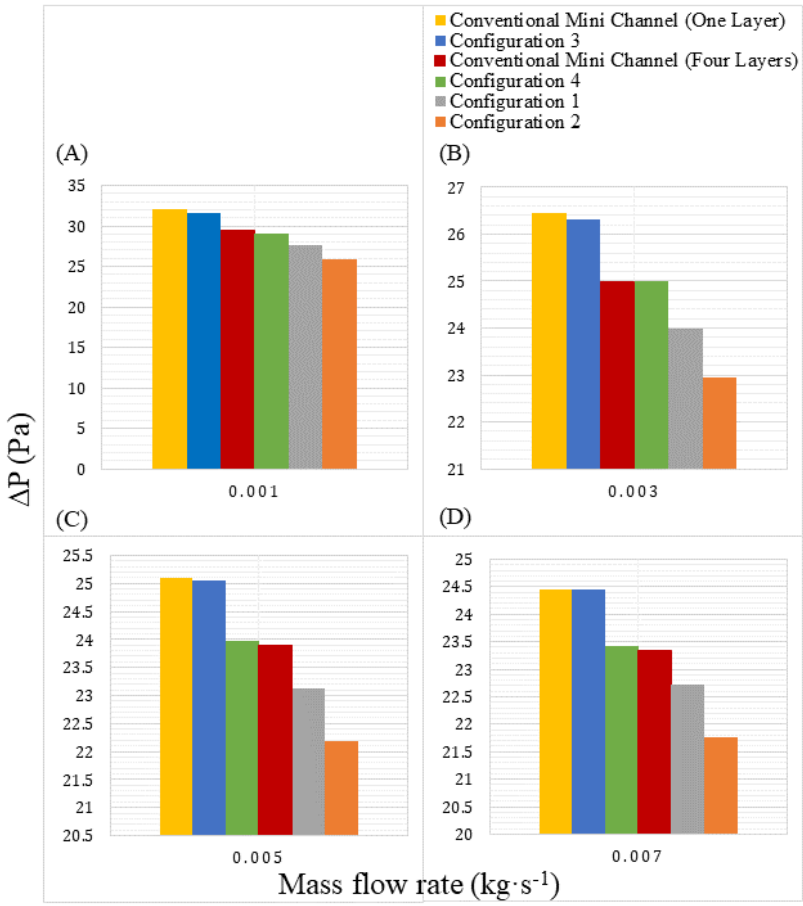

Figure 13. Variation of the pressure drop under CR = 500× at: (**A**) 0.001 kg s^{-1}, (**B**) 0.003 kg s^{-1}, (**C**) 0.0075 kg s^{-1} and (**D**) 0.007 kg s^{-1}.

Moreover, the pressure drop increases as the mass flow rate increases, and it was maximum at 36.32 Pa and 285.85 Pa at a mass flow rate of 0.001 kg s^{-1} and 0.007 kg s^{-1}, respectively. The use of a truncating ratio of 65% has yielded relatively lower pressure drops compared to the conventional MCBHS configurations. The lowest pressure drop was achieved by the first configuration to be 6.42 Pa and 58.01 Pa at 0.001 kg s^{-1} and 0.007 kg s^{-1}, respectively. Moreover, the stacked MCBHS with a truncating ratio of 65% had recorded a lower pressure drop than the other four-layered MCBHS designs and even with respect to the conventional single-layer MCBHS. For instance, at a mass flow rate of 0.001 kg s^{-1} and CR of 500×, the pressure drop was about 13.43 Pa and 17.57 Pa for the second and conventional single-layer MCBHS, respectively.

3.5. Comparative Analysis of Thermal Power to Pumping Power Ratios

It is worth taking into account the scalability of an optimal mini channel configuration; however, in this research the optimum size dimensions of the fins (pitch wise spacing, aspect ratio, width and length) have not been investigated. In fact, the overall thermal resistance can be reduced by increasing the pumping power or employing short fins aspect ratios. However, this may not be the most cost-effective solution. Furthermore, as the hydraulic diameter decreases, for a fixed pressure drop or pumping power, the convection thermal resistance decreases because Nusselt number stays constant. However, the bulk resistance increases because now the flow rate decreases. For unlimited pumping power (or pressure drop), there is no optimum channel dimensions, since the larger size is, the better

the convective heat transfer would be because that will compensate for the increase in bulk thermal resistance especially at small flow rates. The proposed solution for such cases when one set of parameters does not lead for a global optimal solution, the thermal power to the pumping power ratio (dimensionless) is used to perform a designless comparison and judgments between the different configurations under the same fluid amount being flowing per unit of time in the mini channel.

Based on the first law of thermodynamics, the overall performance of the cooling system is dependent on the Ratio of the Thermal power to the Pumping power (RTP). In fact, as higher as the RTP is, as better the cooling configuration would be.

The objective of this section is to map the RTP of each studied MCBHS design at a wide range of Reynolds numbers expressed in this analysis as function of mass flow rates, and under different (CR)s. The RTP will identify the design that promises the minimum overall thermal resistance (maximum actual gained energy) and minimum pumping power at a fixed fluid flow velocity. It is worth noting that the overall thermal resistance for the MCBHS involves the conduction thermal resistance, bulk thermal resistance and convection resistance. In almost all cases of the MCBHS configurations, the conduction thermal resistance can be neglected compared to the other thermal resistances due to the high thermal conductivity and the thin thickness of the heat sink materials. From Figure 14, it was clear that the RTP has the same trend for all (CR)s. In effect, an increase in the water flow rate led to a significant decrease in the RTP.

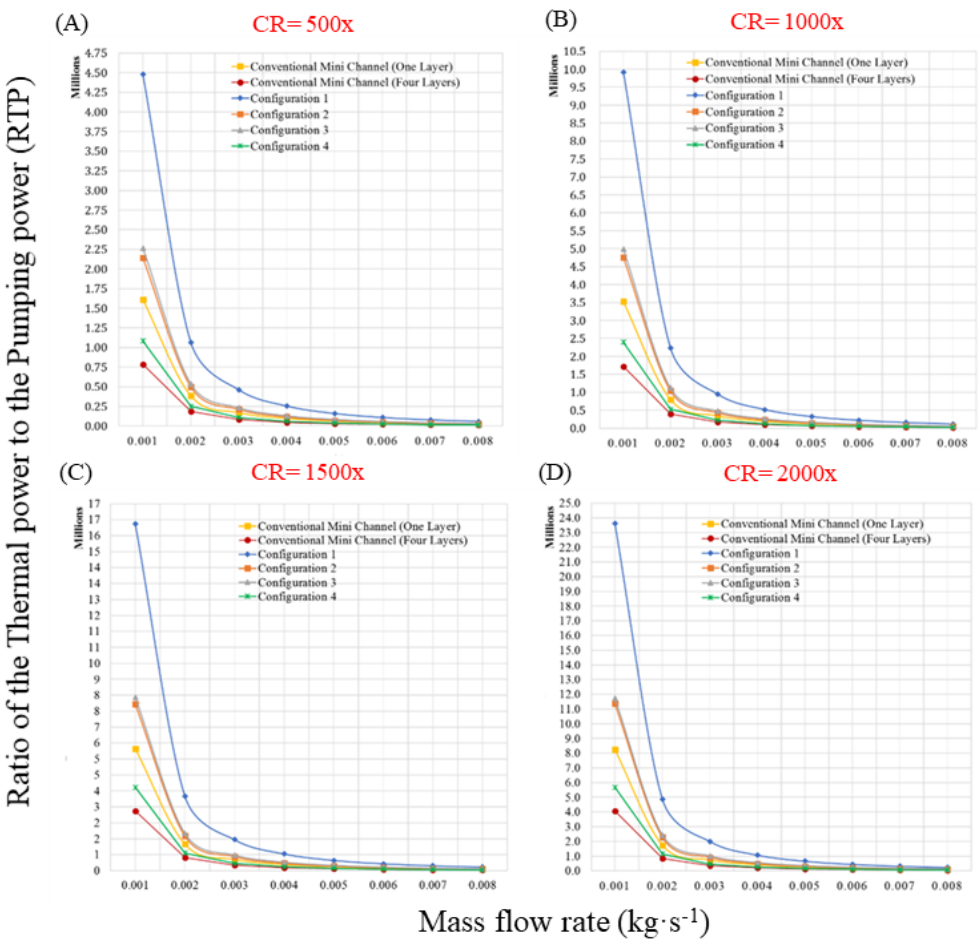

Figure 14. Variation of the RTP against mass flow rate under CR of: (**A**) 500×, (**B**) 1000×, (**C**) 1500× and (**D**) 2000×.

Here, a brief discussion is presented regarding the influence of the mass flow rate on the evolved thermal resistances, which can explain the trending of the (RTP)s under

each prescribed condition. In fact, at small mass flow rates, the single-layer MCBHSs have higher RTP than the stacked MCBHSs due to the highest-convective and bulk thermal resistances at low water velocities. In fact, at small fluid velocity, the flow rate in each mini channel layer decreases, which increases the bulk flow resistance, and the convective heat transfer coefficient is already reduced; therefore, the convective thermal resistance increases. These outcomes engender reduced RTP values for the four-layers MCBHSs. By increasing the fluid flow velocity, the pumping power reduces the bulk and the convective thermal resistance since the Nusselt Number increases accordingly, and therefore the superior actual removed heat by the fluid for the stacked MCBHSs, since they have larger heat transfer areas, will compromise the pressure drop driven by the high flow disturbance and wall skin friction effects because the thermal resistances are made in parallel. For both single-layer and stacked MCBHS, the use of a truncating ratio of 65% has driven the upper hands to achieve higher Ratio of the Thermal power to the Pumping power. The single-layer MCBHS with a truncating ratio of 65% has recorded the maximum RTP of 23.61×10^6 and 233.06×10^3 at a mass flow rate of $0.008\,\mathrm{kg\,s^{-1}}$ and $0.001\,\mathrm{kg\,s^{-1}}$, respectively, under 2000×.

4. Conclusions

The present study attempts to suggest a promising solution to reduce the material cost and time required of the mini channels being employed for the cooling of the high concentration photovoltaic systems. Truncating appropriate fins ratios from the entrance and exit regions of the min channel is adopted to reduce the pressure drop across the channels and the operating energy cost of such cooling mechanism. The proposed designs should meet their functionalities with higher or closed performance to the conventional mini channels. The deduced shortcomings of the present work can be summarized as follows:

- For the single-layer and stacked MCBHS, the use of a truncating ratio of 31% enables achieving minor decrease of the maximum cell temperature, compared to the conventional configurations, but that means a beneficial gain of 31% of the required materials and manufacturing cost of the mini-channel-based heat sink. This outcome has explained the higher recorded electrical efficiencies when using a truncating ratio of 31% for both the single-layer and stacked MCBHS. However, for all investigated configurations, a truncating ratio of 65% is more effective to ensure more surface temperature uniformity distribution.
- For both single-layer and stacked MCBHS, a truncating ratio of 65% qualifies the recording of the highest water outlet temperature and the lowest pressure drops relatively compared to the conventional MCBHS configurations. The highest water temperature has reached up to 52.7 °C by the stacked MCBHS with a truncating ratio of 65% and reached under CR of 2000× and a mass flow rate of 0.001 kg/s.
- For both single-layer and stacked MCBHS, the use of a truncating ratio of 65% has driven the upper hands to achieve higher ratio of thermal power to pumping power. The maximum RTP values have been recorded by the single-layer MCBHS with a truncating ratio of 65% equal to 23.61×10^6 and 233.06×10^3 at a mass flow rate of $0.008\,\mathrm{kg\,s^{-1}}$ and $0.001\,\mathrm{kg\,s^{-1}}$, respectively, under 2000×. Here, it is worth noticing that at high water flow rates, this superiority being achieved by using a truncating ratio of 65% becomes insignificant.

5. Future Work

As avenues of the present work, experimental study emphasizing the performance enhancement and the cost-effectiveness of the proposed designs under the real climate weather conditions of Saudi Arabia will be performed. The economic competitiveness of the proposed HCPVT systems should be compared to that of planar photovoltaic thermal modules available in the market [35]. Future research may examine silicon matrix high-voltage photovoltaic converters [36,37], which are also utilized in concentrator systems, as an alternative to expensive multi-component solar converters due to their high electrical efficiency, low cost and extended service life.The use of a two-component polysiloxane

compound in these solar modules decreases photovoltaic converter deterioration when operating in a concentrated solar flux and at a high operating temperature, which is especially important in Saudi Arabia.

Author Contributions: Conceptualization, F.G.A.-A. and T.M.; methodology, F.G.A.-A. and T.M.; software, A.T.O., T.M. and A.K.A.; validation, A.T.O., A.K.A. and F.G.A.-A.; formal analysis, T.M., N.A.M.H. and R.Z.; investigation, A.T.O., A.K.A. and F.G.A.-A.; resources, the meteorological station implemented at Imam Abdulrahman Bin Faisal University in Dammam city; data curation, the meteorological station implemented at Imam Abdulrahman Bin Faisal University in Dammam city; writing—original draft preparation, A.T.O. and A.K.A.; writing—review, F.G.A.-A. and T.M.; editing, T.M. and R.Z.; visualization, F.G.A.-A., T.M. and N.A.M.H.; supervision, F.G.A.-A. and T.M.; project administration, F.G.A.-A., T.M. and N.A.M.H.; funding acquisition, project number IF-2020-024-Eng. All authors have read and agreed to the published version of the manuscript.

Funding: This research was funded by the Deputyship for Research & Innovation, Ministry of Education in Saudi Arabia grant project number IF-2020-024-Eng.

Data Availability Statement: The data that support the findings of this study are available on request from the corresponding author. The data are not publicly available due to privacy or ethical restrictions.

Acknowledgments: The authors extend their appreciation to the Deputyship for Research & Innovation, Ministry of Education in Saudi Arabia for funding this research work through the project number IF-2020-024-Eng at Imam Abdulrahman bin Faisal University/College of Engineering.

Conflicts of Interest: The authors declare no conflict of interest.

Nomenclature

Abbreviations	
HCPV	High concentration photovoltaic
DNI	Direct normal irradiance
CR	Concentration ratio
MJSC	Multi-junction solar cell
MCBHS	Mini channel-based heat sink
Re	Reynold's number
Symbols	
A_{cell}	Area of the solar cell [m^2]
Q	Thermal power [W]
E	Electric power [W]
$\dot{V}$	Volume flow rate [$m^3\,s^{-1}$]
P	Pressure [Pa]
T	Temperature [°C]
u	Velocity vector [$m\,s^{-1}$]
C_p	Specific heat capacity [$W\,m^{-2}\,°C^{-1}$]
q_{con}	Thermal flux via conduction [$W\,m^{-2}$]
q_{r}	Thermal flux via radiation [$W\,m^{-2}$]
F_{V}	Body force vector [N]
Greek symbols	
η_{sc}	Electrical efficiency of the solar cell
τ	Viscous stress tensor
η_{opt}	Optical efficiency of the solar cell
α_{p}	Thermal expansion coefficient
ρ	Density [$kg\,m^{-3}$]
Subscripts	
f, out	Fluid outlet
f, in	Fluid inlet

References

1. AlOtaibi, Z.S.; Khonkar, H.I.; AlAmoudi, A.O.; Alqahtani, S.H. Current status and future perspectives for localizing the solar photovoltaic industry in the Kingdom of Saudi Arabia. *Energy Transit.* **2020**, *4*, 1–9. [CrossRef]
2. McCrone, A.; Moslener, U.; Destais, F.; Usher, E.; Grüning, C. *Global Trends in Renewable Energy Investment 2016*; Technical Report, Frankfurt School-UNEP Centre and Bloomberg New Energy Finance Report; Frankfurt School of Finance and Management: Frankfurt am Main, Germany, 2016.
3. Maatallah, T.S. A comprehensive study of pin fins cooling channel for a single-cell concentration photovoltaic system under ultra-high concentration ratios. *Int. J. Energy Res.* **2020**, *45*, 4613–4629. [CrossRef]
4. Aldossary, A.; Mahmoud, S.; Al-Dadah, R. Technical feasibility study of passive and active cooling for concentrator PV in harsh environment. *Appl. Therm. Eng.* **2016**, *100*, 490–500. [CrossRef]
5. Khouya, A. Levelized costs of energy and hydrogen of wind farms and concentrated photovoltaic thermal systems. A case study in Morocco. *Int. J. Hydrogen Energy* **2020**, *45*, 31632–31650. [CrossRef]
6. Khouya, A. Performance analysis and optimization of a trilateral organic Rankine powered by a concentrated photovoltaic thermal system. *Energy* **2022**, *247*, 123439. [CrossRef]
7. Jakhar, S.; Soni, M.S.; Gakkhar, N. Historical and recent development of concentrating photovoltaic cooling technologies. *Renew. Sustain. Energy Rev.* **2016**, *60*, 41–59. [CrossRef]
8. Gilmore, N.; Timchenko, V.; Menictas, C. Microchannel cooling of concentrator photovoltaics: A review. *Renew. Sustain. Energy Rev.* **2018**, *90*, 1041–1059. [CrossRef]
9. Xiao, M.; Tang, L.; Zhang, X.; Lun, I.Y.F.; Yuan, Y. A review on recent development of cooling technologies for concentrated photovoltaics (CPV) systems. *Energies* **2018**, *11*, 3416. [CrossRef]
10. Shittu, S.; Li, G.; Zhao, X.; Akhlaghi, Y.G.; Ma, X.; Yu, M. Comparative study of a concentrated photovoltaic-thermoelectric system with and without flat plate heat pipe. *Energy Convers. Manag.* **2019**, *193*, 1–14. [CrossRef]
11. Alzahrani, M.; Baig, H.; Shanks, K.; Mallick, T. Estimation of the performance limits of a concentrator solar cell coupled with a micro heat sink based on a finite element simulation. *Appl. Therm. Eng.* **2020**, *176*, 115315. [CrossRef]
12. Anand, S.; Senthil Kumar, M.; Balasubramanian, K.R.; Krishnan, R.A.; Maheswari, L. An experimental study on thermal management of concentrated photovoltaic cell using loop heat pipe and heat sink. *Heat Transf. Asian Res.* **2019**, *48*, 2456–2477. [CrossRef]
13. Ahmed, A.; Shanks, K.; Sundaram, S.; Mallick, T.K. Theoretical investigation of the temperature limits of an actively cooled high concentration photovoltaic system. *Energies* **2020**, *13*, 1902. [CrossRef]
14. Ahmed, A.; Zhang, G.; Shanks, K.; Sundaram, S.; Ding, Y.; Mallick, T. Performance evaluation of single multi-junction solar cell for high concentrator photovoltaics using minichannel heat sink with nanofluids. *Appl. Therm. Eng.* **2021**, *182*, 115868. [CrossRef]
15. Rastan, H.; Abdi, A.; Hamawandi, B.; Ignatowicz, M.; Meyer, J.P.; Palm, B. Heat transfer study of enhanced additively manufactured minichannel heat exchangers. *Int. J. Heat Mass Transf.* **2020**, *161*, 120271. [CrossRef]
16. Deng, Z.; Shen, J.; Dai, W.; Liu, Y.; Song, Q.; Gong, W.; Ke, L.; Gong, M. Flow and thermal analysis of hybrid mini-channel and slot jet array heat sink. *Appl. Therm. Eng.* **2020**, *171*, 115063. [CrossRef]
17. Xiao, H.; Liu, Z.; Liu, W. Conjugate heat transfer enhancement in the mini-channel heat sink by realizing the optimized flow pattern. *Appl. Therm. Eng.* **2021**, *182*, 116131. [CrossRef]
18. Anwar, M.; Tariq, H.A.; Shoukat, A.A.; Ali, H.M.; Ali, H. Numerical study for heat transfer enhancement using cuo-water nanofluids through mini-channel heat sinks for microprocessor cooling. *Therm. Sci.* **2020**, *24*, 2965–2976. [CrossRef]
19. Barrau, J.; Chemisana, D.; Rosell, J.; Tadrist, L.; Ibañez, M. An experimental study of a new hybrid jet impingement/micro-channel cooling scheme. *Appl. Therm. Eng.* **2010**, *30*, 2058–2066. [CrossRef]
20. Ali, A.; Abo-Zahhad, E.M.; Elqady, H.I.; Rabie, M.; Elkady, M.F.; El-Shazly, A.H. Impact of microchannel heat sink configuration on the performance of high concentrator photovoltaic solar module. *Energy Rep.* **2020**, *6*, 260–265. [CrossRef]
21. Ali, A.Y.M.; Abo-Zahhad, E.M.; Elqady, H.I.; Rabie, M.; Elkady, M.F.; Ookawara, S.; El-Shazly, A.H.; Radwan, A. Thermal analysis of high concentrator photovoltaic module using convergent-divergent microchannel heat sink design. *Appl. Therm. Eng.* **2021**, *183*, 116201. [CrossRef]
22. Khoshvaght-Aliabadi, M.; Hormozi, F.; Zamzamian, A. Experimental analysis of thermal-hydraulic performance of copper-water nanofluid flow in different plate-fin channels. *Exp. Therm. Fluid Sci.* **2014**, *52*, 248–258. [CrossRef]
23. Abo-Zahhad, E.M.; Ookawara, S.; Radwan, A.; El-Shazly, A.H.; ElKady, M.F. Thermal and structure analyses of high concentrator solar cell under confined jet impingement cooling. *Energy Convers. Manag.* **2018**, *176*, 39–54. [CrossRef]
24. Abo-Zahhad, E.M.; Ookawara, S.; Radwan, A.; El-Shazly, A.H.; Elkady, M.F. Numerical analyses of hybrid jet impingement/microchannel cooling device for thermal management of high concentrator triple-junction solar cell. *Appl. Energy* **2019**, *253*, 113538. [CrossRef]
25. Abo-Zahhad, E.M.; Ookawara, S.; Esmail, M.F.; El-Shazly, A.H.; Elkady, M.F.; Radwan, A. Thermal management of high concentrator solar cell using new designs of stepwise varying width microchannel cooling scheme. *Appl. Therm. Eng.* **2020**, *172*, 115124. [CrossRef]
26. Sabry, M. Temperature optimization of high concentrated active cooled solar cells. *NRIAG J. Astron. Geophys.* **2016**, *5*, 23–29. [CrossRef]

27. Tan, W.C.; Chong, K.K.; Tan, M.H. Performance study of water-cooled multiple-channel heat sinks in the application of ultra-high concentrator photovoltaic system. *Sol. Energy* **2017**, *147*, 314–327. [CrossRef]
28. Bird, R.B.; Stewart, W.E.; Lightfoot, E.N. *Transport Phenomena*, 2nd ed.; John Wiley & Sons, Inc.: Hoboken, NJ, USA, 2002.
29. Burmeister, C.L. *Convective Heat Transfer*, 2nd ed.; John Wiley & Sons Inc.: Hoboken, NJ, USA, 1993.
30. AlFalah, G.; Maatallah, T.S.; Alzahrani, M.; Al-Amri, F.G. Optimization and feasibility analysis of a microscale pin-fins heat sink of an ultrahigh concentrating photovoltaic system. *Int. J. Energy Res.* **2020**, *44*, 11852–11871. [CrossRef]
31. Ahmed, F.E.; Lalia, B.S.; Hashaikeh, R.; Hilal, N. Alternative heating techniques in membrane distillation: A review. *Desalination* **2020**, *496*, 114713. [CrossRef]
32. Li, Q.; Beier, L.J.; Tan, J.; Brown, C.; Lian, B.; Zhong, W.; Wang, Y.; Ji, C.; Dai, P.; Li, T.; et al. An integrated, solar-driven membrane distillation system for water purification and energy generation. *Appl. Energy* **2019**, *237*, 534–548. [CrossRef]
33. Sharif, M.K.A.; Al-Abidi, A.A.; Mat, S.; Sopian, K.; Ruslan, M.H.; Sulaiman, M.Y.; Rosli, M.A.M. Review of the application of phase change material for heating and domestic hot water systems. *Renew. Sustain. Energy Rev.* **2015**, *42*, 557–568. [CrossRef]
34. Nikbakhti, R.; Wang, X.; Chan, A. Performance analysis of an integrated adsorption and absorption refrigeration system. *Int. J. Refrig.* **2020**, *117*, 269–283. [CrossRef]
35. Kharchenko, V.; Panchenko, V.; Tikhonov, P.V.; Vasant, P. Cogenerative PV thermal modules of different design for autonomous heat and electricity supply. In *Handbook of Research on Renewable Energy and Electric Resources for Sustainable Rural Development*; IGI Global: Hershey, PA, USA, 2018; pp. 86–119.
36. Panchenko, V.; Izmailov, A.; Kharchenko, V.; Lobachevskiy, Y. Photovoltaic Solar Modules of Different Types and Designs for Energy Supply. *Int. J. Energy Optim. Eng.* **2020**, *9*, 74–94. [CrossRef]
37. Panchenko, V. Photovoltaic Thermal Module With Paraboloid Type Solar Concentrators. *Int. J. Energy Optim. Eng.* **2021**, *10*, 1–23. [CrossRef]